International Journal of
INTELLIGENT SYSTEMS AND APPLICATIONS IN ENGINEERING
ISSN:2147-6799 www.ijisae.org Original Research Paper

# A Novel Modified Marine Predator Algorithm (MMPA) based Automated Atrial Fibrillation Detection (AAFD) System using ECG Signals

**Sreenivasulu Ummadisetty* and Madhavi Tatineni**

**Submitted**: 26/08/2023 **Revised**: 21/10/2023 **Accepted**: 03/11/2023

**Abstract:** The most common type of arrhythmia that can modify the heart's rhythms and potentially impact the morphology of ECG tracings is called Atrial Fibrillation (AF). The recent statistical reports indicate that nearly 1% of people around the world are affected by AF. The major goal of this article is to develop a method for automatically detecting AF using transient single lead ECG readings. Heart rate variability (HRV) and frequency analysis are used for feature extraction. This study's innovative contribution is the use of a Modified Marine Predator Algorithm (MMPA) to identify AF in brief ECG data. After feature selection, the AF classification is performed with the use of Support Vector Machine (SVM) classifier. It segregates the classes into the types of Normal & Arrhythmia (NA), Others & Arrhythmia (OA), Normal & Others (NO), and Normal, Others & Arrhythmia (NOA). The outcomes were verified and compared by using a publicly accessible data set made up of brief ECG recordings generated by the existing, SVM, Genetic Algorithm (GA-SVM), and Modified Moth-Flame (MMF-SVM) techniques. Under noise levels between 0 and 30 dB, classification accuracy for N versus A ranges from 96% to 99%. The maximum accuracy of 99.8% is attained for N versus A versus O. The acquired experimental results indicate that, for relatively brief ECG recordings, HRV is effective and reliable for AF identification.

***Keywords:*** *Atrial Fibrillation (AF), Electrocardiogram (ECG), Modified Marine Predator Algorithm (MMPA), Support Vector Machine (SVM), Heart rate variability (HRV), and Spectral Features.*

## 1. Introduction

The most prevalent supraventricular cardiac arrhythmia is a condition called atrial fibrillation (AF) [1, 2], which is associated with a substantial premature mortality in those who experience it. Cases of AF are caused by periodic ventricular excitations, which damage the heart's functioning and raise the possibility of a stroke or cardiac arrest. A dangerous and prevalent pathophysiological mechanism that results from aberrant electrical impulses is arrhythmia. Due to their high incidence rates and mortality rates [3], AF has a significant impact on patients' health in all types of arrhythmias. It has comparable clinical characteristics and are not easily sensed by the human body. Typically, the AF [4] is an aberrant electrical function of the heart, because the chambers of the atria cannot pump blood normally. Since the chambers of the atria cannot pump blood normally, AF is an aberrant electrical function of the heart. Atrial tachycardia, which is characterized by a heart rate of in excess of 100 beats per minute, can be a symptom that may be present. When AF is present [5, 6], the P-wave has been substituted by a continuous, irregular F-wave, and RR intervals are entirely erratic. It is crucial to address the causes and symptoms of AF, since it may vary from person to person, and any deeper medical problems in order to avoid a stroke. Treatment options include drugs, electric cardiac arrest, and removal of the heart's afflicted region, implanted pacemakers, changes in behavior, and a reduction in weight. Successful medication requires prompt and systematic prediction, diagnosis, and classification of AF [7]. This disease is commonly affected the elderly people, and the world health reports indicate that nearly 18 million people are suffering by AF. Because of this, it is the focus of much research in both the medical and technical disciplines. Prediction, identification, and discovery are the three axes that are the focus of the more recent research. Due to the fact that AF is frequently asymptomatic and that its episodes of symptoms are frequently short, its automated early identification is a very challenging but clinically crucial task to enhance AF treatment and lower patient risks [8]. Moreover, early detection could therefore be highly helpful in avoiding fatalities. Also, analyzing the electrical activity of the cardiovascular system can be used to find AF. The signals of the Electrocardiogram (ECG) depict the atria and ventricles' depolarization and repolarization. Recent years have seen a rise in the use of Artificial Intelligence (AI) to deliver efficient pattern recognition methods for diagnostic systems [9, 10] across numerous industries, particularly in the healthcare sector. The early detection of AF symptoms and the prognosis of AF events are both made possible by AI [11]. As a result, many significant health issues can now be avoided.

Identifying abnormalities and classifying or predicting them

*Department of EECE, GITAM (Deemed to Be University), Visakhapatnam, Andhra Pradesh, India.*
**Corresponding author: summadis@gitam.edu*

are the primary objectives of ECG signal analysis. This can be done by using computer-aided diagnosis systems [12, 13], including those that employ AI mechanisms. The extraction of ECG traits utilizing flexible approaches, like wavelet transformation, is essential for identifying anomalies. The potency of AF treatment options will be constrained by the lingering problem of prompt and automated AF identification. Machine learning (ML) [13] approaches have gained a lot of popularity in recent years for use in dealing with problems from a variety of industries, including medical. This popularity is a result of ML's ability to handle issues that are challenging to address conventionally due to the presence of unpredictable rules. These techniques can address a wide range of issues because of the characteristics of learning and the generalization of information. In several scientific domains [14], artificial intelligence techniques are quite effective. The positive effects of ML are found in the traits they inherited from biological counterparts, such as information interpretation, learning, and the usage of imperfect terminology. Numerous research have shown that adding machine learning features and optimization approaches to the classifier would improve system performance and result in more precise classification results. We can show that different neural networks may successfully extract complex nonlinear properties from the original data without the requirement for human involvement, despite the fact that the aforementioned research can successfully address the classification problem for AF. Learning the reasoning behind the ECG signal features with the high accuracy required for monitoring is still difficult, though. Based on the survey [15, 16], it is determined which issues the previous works have, including lack of efficiency, zero-frequency problem, low accuracy, an inability to handle huge datasets, and longer training times. Therefore, the proposed study promotes the development of novel optimization and classification models for an automated AF detection. Following are the paper's primary research goals:

- In order to increase classification accuracy, various signal features, including spectral and HRV-based features, are extracted.
- The Modified Marine Predator Algorithm (MMPA) is designed to select the most pertinent characteristics from the list of accessible features in the best possible way.
- The Support Vector Machine (SVM) classification algorithm is created to precisely detect and forecast the AF from the provided ECG signals based on its best features.
- In this study, a comprehensive simulation and comparative studies are conducted to validate and test the performance of the suggested system.

This proposed work's novel contribution is the creation of a highly effective and qualified methodology for detecting AF from the provided ECG signals. The dynamic properties of the cardiac activity have been analyzed in this framework using the HRV-based feature extraction methodology. The HRV model's high level of robustness contributes to improved detection confidence and accuracy. Additionally, the moth flame optimization process is utilized to choose the features from the collection of accessible features in the best way possible, which boosts training rates and lowers classification false prediction rates. By using the refined collection of characteristics, an improved SVM model is used to precisely detect AF.

## 2. Related Works

*Ebrahimi, et al* [17] conducted a detailed review on various deep learning techniques used for the detection of arrhythmia from ECG signals. The study indicates that the deep learning techniques are widely applied in the healthcare applications for the disease identification and recognition. In this survey, the techniques such as Deep Belief Network (DBN), Gated Recurrent Unit (GRU), Recurrent Neural Network (RNN), and Convolutional Neural Network (CNN) are used for arrhythmia classification. *Wang, et al* [18] utilized a modified bi-directional LSTM network classification algorithm for the detection of atrial fibrillation from ECG signals. The authors suggested an MB-LSTM network using an attribute recalibration method that allows the classification of AF and AFL signals while surpassing various modern methods on open databases. The suggested model can be seen as an enhanced version of the current LSTM and B-LSTM models. RNN, on the other hand, struggle to simulate feature information from the past as a result of the restricted memory and underlying structure and is susceptible to explosion of gradients and shrinking issues when sequence interval grows. *Chen, et al* [19] implemented a CNN integrated LSTM technique to automatically detect arrhythmia from the ECG signals. The most popular supervised model that appears to be efficient in learning intricate structures is multi-layer perceptron. The feed-forward connections between the layers of neurons that make up the MLP architecture vary. Each neuron is made up of the weighted total of its inputs following the time they have been through a process that is not linear.

*Plawiak, et al* [20] implemented an ensemble based classification algorithm for identifying arrhythmia from the given ECG signals. In this study, the MIT-BIH dataset has been used to validate and assess the outcomes of the studied models. Moreover, the normalization techniques, cross validation approaches, layered learning and optimized classification approaches are used to accurately recognize the disease. The suggested framework comprises the operations of normalization, QRS complex detection,

spectral density based feature extraction, GA based feature selection, and cross validation. However, the classification performance is not up to the mark, which could be the main problem of this work. *Murat, et al* [21] conducted a comprehensive review to examine various deep learning techniques used for the detection of heart beat. Here, the CNN based representative learning methodology is used for identifying disease with better accuracy. *Ukil, et al* [22] deployed a new technology, named as, AFSense for the identification of cardiac arrhythmia with high detection rate. The authors aim to enhance an automatic detection process of arrhythmia by optimizing the learning at the time of classification. *Ahmad, et al* [23] intended to develop a low cost health monitoring system for the early detection of Atrial fibrillation. In the suggested framework, the digital filtering method was integrated to obtain better prediction performance. For this study, the MIT-BIH public dataset has been utilized that comprises the long-term of ECG recording signals. In order to determine the efficacy of the suggested methodology the RR interval minimum and maximum time are estimated.

*Lyakhov, et al* [24] utilized a wavelet based preprocessing methodology integrated with the neural network classifier for the better detection of Atrial fibrillation. Here, the symlet wavelet filtering technique is mainly used to preprocess the input ECG signal by computing the spectral entropy functions. Any digital signal will be corrupted by disruptions of different noises. It is challenging for both experts and systems using artificial intelligence to analyze the data due to the noise on the ECG signals. Through signal preprocessing, the ECG can be ready for additional analysis. After preparing signals, both the spectral entropy and instantaneous frequency are estimated for an effective classification. Moreover, the LSTM classification method is used to categorize the healthy and AF signals from the preprocessed signals. However, the suggested system took more time to detect the disease, which affects the efficiency of the AF detection framework. *Wang, et al* [25] utilized an Elman NN classification technique for developing an automated AF detection. In this study, the detection of both AF and AFL are concentrated by the authors with high accuracy. The advantages of the suggested framework are better reliability and efficiency, but the training complexity of this system is quite complex. *Tutuko, et al* [1] introduced an automated AF detection system using the CNN integrated LSTM technique for AF identification. Here, the training and testing performance of the suggested model was validated and compared by using the set of model evaluation parameters. The suggested mechanism has the better ability to handle complex datasets with accurate prediction results.

## 3. Proposed Methodology

This study seeks to build an effective and reliable AAFD approach for processing data collected from wearable or portable devices in noisy conditions. The information gathered from the gadgets is typically unreliable. Instead of a clear portion of long signal, it could have been anticipated that the recording signals would be available in smaller slices. Additionally, portable gadgets cannot be attached to patients and will not function in the same way as wearable technology. The length of the recording typically relies on the patient's behaviors, making it impossible for the developers to analyze the data. Even though morphological factors like PR/ST intervals and QRS complex length are physiologically sound and therapeutically important, they were not preferred since they were unsuitable for the aforementioned situations. Due to its relative invulnerability to all other features, the R peak in an ECG signal is typically the dominating fiducial point. The characteristic waves or other fiducial points may not be very helpful if there are no identifiable R peaks in any segment of the ECG. For both low and moderate noise levels, R peak can be recognized with good accuracy and confidence. Due to their robustness in noisy circumstances, HRV-based traits were therefore taken into consideration for the dynamic properties of cardiac activity. Fig 1 shows the general structure of the proposed technique.

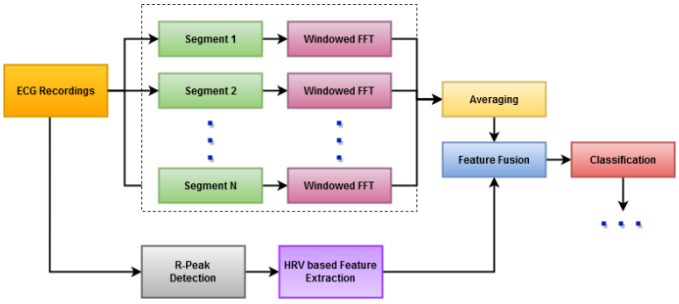


**Fig 1.** Overall framework model

### 3.1. Dataset Description

The data required for the current endeavor is obtained from the publicly accessible dataset named as, Computing in Cardiology Challenge (CinC) released in 2017. It consists of brief ECG recordings that are obtained with a single lead and have a total length of 9 seconds to more than 1 minute (8528 records). These recordings are classified by clinical cardiologists as having normal rhythm (N), atrial fibrillation (AF), other arrhythmias (O), and noisy (~). The dataset distribution and representative recordings are displayed in Table 1 and Figure 2. Around 60% of the recorded data from the labelled dataset is classified as normal rhythm, 9% as AF events, and 28% as arrhythmias other than atrial fibrillation. The remaining 3% of the data have been determined to be excessively noisy.

**Table 1.** Dataset distribution of the sample recordings

| *Type* | *# Recordings* | *% portion* |
|---|---|---|
| Normal Rhythm (N) | 5076 | 59.52% |
| Atrial Fibrillation (AF) | 758 | 8.89% |
| Other Arrhythmias (O) | 2415 | 28.32% |
| Noisy (~) | 279 | 3.27% |
| Total | 8528 | 100% |

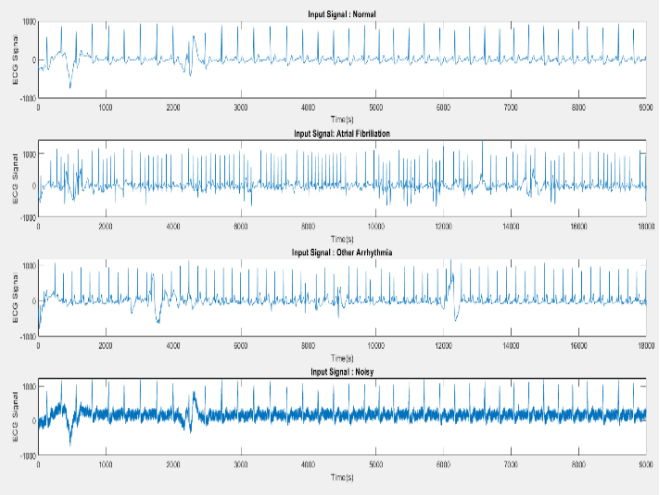


**Fig 2.** Sample ECG signal

### 3.2. Feature Extraction

In this study, two different feature extraction techniques are used for effective AF identification and classification, which includes HRV based features and spectral features. The extraction of HRV-based characteristics is the very first step in the detection of the R peak. Here, the average HR value is estimated by using $HR = 60 \times \frac{N.f}{L}$ in terms of beats/mins, where N indicates the number of R peaks, f denotes the sampling signal frequency in Hz, and L represents the length of the recording. Then, the N number of R peaks having N-1 intervals and the sequence of RRI is represented in the form of $RRI = [RR_1, RR_2, \ldots . RR_{N-1}]$. Heart rate variability (HRV) is referred to the the fluctuation in heart rate from beat to beat or the length of the R-R interval, serves as a typical clinical and research tool. The energy distribution and functions of the autonomous nervous system (ANS) are related to the frequency-domain of HRV. Plotting the PSD's logarithm against the frequency's logarithm yields a power-law connection in the power spectrum density (PSD) of HRV. Sympathetic-vagal equilibrium is interpreted by this PSD. The original ECG signal and RRI sequence are depicted in Fig 3.

If the heartbeat has a rigid steady rhythm, HRV cannot be detected. Interpolation & resampling and the Lomb-Scargle Periodogram are the two approaches that are most frequently employed to prevent unevenness in the time domain. The disadvantage of the approaches mentioned above is that any signal, whether it is evenly distributed or not, can be sampled under the fictitious premise of a continuous random process. Even if time variation occurs, it becomes challenging to measure HRV in a unit of time if it is seen as a function of time. Consequently, a better model is required to prevent the use of probability distribution-based explicit or implicit interpolation techniques. The analytically determined values from the formula with hypothesized coefficients are used in the point procedure. Moreover, the point procedure based on HRV analysis has two benefits. It does not necessitate the derivation of new measures, and it does away with subpar interpolation.

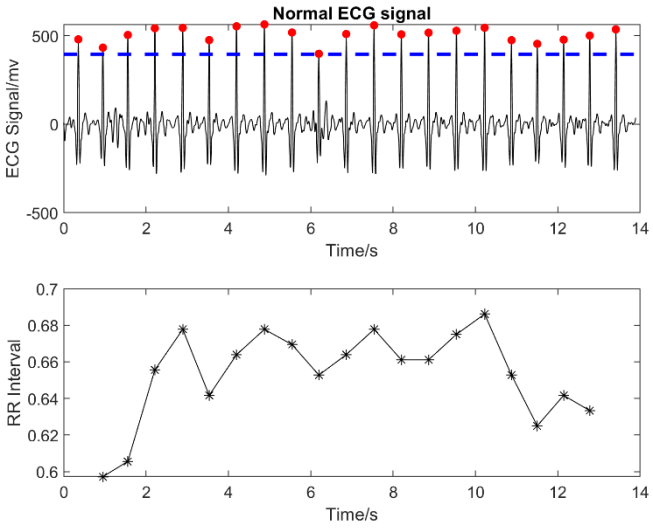


**Fig 3.** HRV obtained from input ECG signal (a). Original input and (b). RR interval

Only unacceptably low frequency resolution will be available to wearable devices. The European Hematology Association (EHA) advised that a recording should be no longer than five minutes. However, in this instance, the recording duration varies from 9 seconds upwards to more than 1 minute, which is far shorter than what EHA advises. The uncertainty principle of quantum physics, which applies to signal processing, argues that a given signal's time and frequency resolution may not be arbitrarily high concurrent. The normalized energy distribution value for the given signal s(t) on the time axis as $\left(\int_{-\infty}^{\infty}|s(t)|^2 dt = 1\right)$, which is mathematically represented in below:

$$\left(\int_R t^2|s(t)|^2 dt\right).\left(\int_R f^2|\hat{s}(f)|^2 df\right) \leq \frac{1}{16\pi^2} \quad (1)$$

Where, $\hat{s}(f)$ denotes the Fourier transform of s(t). However, the energy concentration signal in the corresponding frequency domain is substantially worse than the signals obtained from RRI sequences, which are compactable in the time domain. The estimation of RRI sequences with high energy concentrations is used in this research effort instead

of direct power spectrum density because of the aforementioned reasons. RRI sequences' first-order differences were organized to form a patterned matrix. In a 2-D plane, a Poincare Plot was created to map several descriptors in the patterned matrix. These Poincare plots have the advantage of characterizing the comprehensive dynamic information given. Here, RRI's first-order difference is represented by $dRR_i = RR_i + 1 - dRR_i$. Hermann Hankel matrix is a square matrix of nth order that may be described by either its initial row or column. This signal-derived Hankel matrix is helpful for time-frequency encoding and dissecting non-stationary signals. The Hankel matrix (A) is represented by the following:

$$H = \begin{bmatrix} a_1 & a_2 & a_3 & \dots & a_n \\ a_2 & a_3 & a_4 & \dots & a_1 \\ . & . & . & . & . \\ . & . & . & . & . \\ . & . & . & . & . \\ a_{n-1} & a_n & a_1 & \dots & a_{n-2} \\ a_n & a_1 & a_2 & \dots & a_{n-1} \end{bmatrix} \quad (2)$$

Each rising skew-diagonal from left to right is a constant in the Hankel matrix known as Hermitian symmetry. Consequently, it is diagonalized as represented in the following equation:

$$H = U * DU \quad (3)$$

All of the eigenvalues of H are organized along the diagonal line of the diagonal matrix D, and * stands for the conjugate transpose. It was discovered that the square matrix H's spectral radius also happens to be its central symmetry and that it has the biggest absolute value of the eigenvectors that make up its U bases in the Fourier domain. As a result, the eigenvalues are all listed in ascending order. The matrix U is a permutation matrix, a binary square matrix with exactly one entry of 1 in each row and column and 0s in all other locations. U and U*'s rows and columns were permuted in the appropriate ways. The matrix U contains a non-zero entry in the $i_{th}$ column is denoted as $I_i$, $i \in 1, 2, \dots\dots, \frac{n}{2}$; the Hankel distance (HankDist) is defined by the following model:

$$HankDist = \frac{4}{n^2} \sum_{i=1}^{\left[\frac{n}{2}\right]} |I_i - i| \quad (4)$$

The only sinusoidal sequences that appear on the diagonal and anti-diagonal lines in the feature maps are those with non-zero entries. Such a Hankdist's obtained matrix series will be 0. The HankDist is big for feature maps with erratic scatter. Both RRI and dRR are used to determine the HankDist. The standard descriptors in the Poincare plot comprises the linear descriptors such as $SD_1$, $SD_2$ and $SD_{ratio} = SD_1/SD_2$ of the RRI sequence. The (RR1, RR2) pair is displayed against RRi for RRI consecutive pairs. The straight-line y = x is where the data points from the normal RRI in the created Poincare plot lie, and these data points are used to generate an ellipse. Long-term dispersion is replicated by the ellipse's long axis ($SD_1$). In contrast, the short axis ($SD_2$) reflects the dynamics of cardiac activity as well as the short-term distribution of RRI variation. Moreover, the data points are 45° rotated in the clockwise direction for extracting $SD_1$ and $SD_2$, and $(x, y)^T$ is represented by $(RR_i, RR_{i+1})^T$ where i = 1, 2, ….., N-1 then,

$$\begin{bmatrix} x' \\ y' \end{bmatrix} = \begin{bmatrix} cos\frac{\pi}{4} & sin\frac{\pi}{4} \\ -sin\frac{\pi}{4} & cos\frac{\pi}{4} \end{bmatrix} \cdot \begin{bmatrix} x \\ y \end{bmatrix} \quad (5)$$

The new data points were donated with $(x', y')^T$ whereas the variance along x' axes is computed as $SD_1$, and $SD_2^2 = 2.Var(RR) - SD_1^2$. Although the descriptors (SD1, SD2) are a linear combination of the fundamental statistics of the original RRI sequence, the Poincare plot is discovered as a nonlinear analysis tool. The original RRI series is subjected to the second-order statistics in order to rule out nonlinearity. The fact that the aforementioned descriptors were invariant suggested that RRI had a limited ability to reflect the order structure. After any conceivable delay-embedding, the area occupied by three successive RRI pairs is utilized to calculate the term generation. The area occupied by $((RR_i, RR_{i+1}) \rightarrow (RR_{i+1}, RR_{i+2}) \rightarrow (RR_{i+2}; RR_{i+3}))$ is denoted with A(i) shown in below:

$$A(i) = \begin{vmatrix} RR_i & RR_{i+1} & 1 \\ RR_{i+1} & RR_{i+2} & 1 \\ RR_{i+2} & RR_{i+2} & 1 \end{vmatrix} \quad (6)$$

Then, the CCM of the normalized area is computed as shown in the following model:

$$CCM = \frac{1}{K\pi SD_1.SD_2} . \sum_{i=1}^{K} A(i) \quad (7)$$

In addition to RRI, it is reasonable to anticipate power spectrum distribution (PSD) characteristics with frequency interpretation of components. However, this PSD from the difference between RRI sequences (δRR) demonstrates that it was unable to offer a meaningful variance with respect to white noise. However, it has been found that δRR can tell AF apart from a regular beat. The fact that HRV-based features only include information on heart activities in the sketch is one of their key drawbacks. ECG has intricate morphology. The characteristic waves (CW) should not be characterized in the time domain because of its noise sensitivity; however, the frequency domain has a very stable structure. The Periodogram approach is very slightly altered by the estimation of the Welch PSD. Welch PSD estimates reduced variance more accurately than the Periodogram approach, but at the penalty of lesser frequency resolution. Assume there is a single, homogeneous ECG signal with length N. This signal is separated into M equal segments of length L, either overlapping or not. Moreover, the

overlapping with D is defined as shown in the following model:

$$L + (M - 1)(L - D) = N \quad (8)$$

Then, the windowed Discrete Fourier Transformation (DFT) is estimated for each and every segmented $X_k(i), i = 0,1,2 \ldots L - 1$ as shown in the following equation:

$$\hat{P}_k(n) = \frac{1}{L} \sum_{i=0}^{L-1} X_k(i) W(i) e^{-2\Pi j i \frac{n}{L}}, \; k = 1,2, \ldots, M \quad (9)$$

Where, W(i) indicates the window function used to reduce the frequency leakage. At last, the spectral estimation is scaled into $\left[\frac{-1}{2}, \frac{1}{2}\right]$, which is the normalised average of all the M Periodogram and is defined by using the following models:

$$\hat{p}\left(\frac{n}{L}\right) = \frac{1}{M} \sum_{k=1}^{M} \frac{|L.\hat{P}_k(n)|^2}{W_0}, n = 1,2, \ldots, \frac{L}{2} \quad (10)$$

Where, $W_0$ indicates the energy of the window function estimated by the following model:

$$W_0 = \sum_{i=0}^{L-1} |W(i)|^2 \quad (11)$$

Therefore, the frequency resolution is reduced from $\frac{N}{2}$ to $\frac{L}{2}$, and also its variance is reduced by a factor up to M. Moreover, the order of magnitude of N is up to $10^3 – 10^4$. If M's order of magnitude is about $10^1$, the sampling frequency about 300 Hz is considered in this case, since the power spectrum can be distributed in the range of 0-150 Hz and still it has a resolution level of about 1 frequency point/Hz.

### 3.3. Modified Marine Predator Algorithm (MMPA) for Feature Selection

The choice of features is crucial since it prevents overfitting and aids in choosing the most discriminative features from the available feature set. The performance of the training set has an impact on the model's resilience, while the size of the overall model has an impact on the speed of inference. The aforementioned characteristics have thus far been measured using various interval scales. As a result, it is necessary to adopt a model-free feature selection approach. Maximum Relevance Minor Redundancy (MRMR), which is based on mutual information, is used in this work. This model can maximize relevance while eliminating redundancies between the features and the targets (labels), as its name suggests. The relevance and redundancy are estimated using the mutual information. Here, the set of original features and chosen features are represented by Ω and S respectively. The feature selection is mainly used to obtain the optimal subset S as represented in the following model:

$$\underset{S \subseteq \Omega}{arg\,max}\, I(S_m, t) \quad (12)$$

Where, t indicates the the targets labels, I (. , .) as the mutual information estimation and | . | as the cardinality operator. It is thought to be impractical to choose a simple selection method that employs an exhaustive search to determine the combinatorial subset S. Additionally, for the high dimensional variable, it is challenging to estimate the mutual information. In the proposed work, the Modified Marine Predator Algorithm (MMPA) optimization technique for choosing the most relevant features. It is one of the nature-inspired algorithm and more suitable for solving complex optimization issues. Predators adopt the common foraging tactic known as the Brownian and Lévy random movement, which is inspired by the MPA. However, environmental problems like the creation of eddies or the effects of fish aggregating devices (FADs) make up the things that affect how marine predators behave. A more evenly dispersed beginning population has been produced through opposition-based learning, and the chaotic map aids in balancing the trade-off among the prospecting and extraction stages. In each cycle, the self-adaptive population approach automatically modifies the population size, which facilitates quickening convergence. As a consequence, a control parameter is required for determining the population size. The crucial thing to remember is that selecting the population size for the event solving issues is a complicated and challenging task. In each cycle, the self-adaptive population modifies the population's size. Its key advantage is that the population size is automatically adjusted throughout each iteration, relieving the user from having to pay attention to this. A strategy called a chaos map substitutes unexpected chaotic variables for random ones. In comparison to probability-based randomised hunts, they carry out straightforward searches at a faster pace of convergence. Because of the chaotic sequence's dynamic behavior, the optimization procedures assists better exploration in the search space. In this technique, the set of populations are initialized at the beginning with the upper and lower bound values. Then, the fitness of each population is determined according to the fitness function. Based on the best fittest value, the top member is selected, and its vector is computed for constructing the elite matrix. Then, the prey position updation is performed, and also elite and memory update are executed consequently. Finally, the best optimal position of prey is updated, and the process has been repeated until reaching the maximum number of iterations. The algorithmic steps included in the MMPA are given below:

***Algorithm 1 – MMPA based Feature Selection***

Step 1: Initialize search agents (prey) population i.e., different combination of features sets i=1,2,….n;

Step 2: Calculate the fitness (MRMR with SVM classification accuracy), construct the Elite matrix (combinational features which got more accuracy) and accomplish memory saving;

Step 3: if $iter < Max_{iter}/3$

Update prey;

Else if $\frac{Max_{iter}}{3} < Itr < 2 \times \frac{Max_{iter}}{3}$

For the first half of the populations$i = 1,2 \ldots \frac{n}{2}$

Update prey;

Else if $Iter > 2 \times \frac{Max_{iter}}{3}$

Update prey based on the searching combinations;

End if;

Step 4: Set $R = rand$

While $Iter < \frac{1}{3} Max_{Iter}$

If $R > 0.5$

$$\overrightarrow{stepsize_i} = \left(\overrightarrow{Elite_i} - \vec{R}_B * \overrightarrow{Prey_i}\right) * \vec{R}_B, i = 1, \ldots n$$

$$\overrightarrow{Prey_i} = \overrightarrow{Prey_i} + P.\vec{R} * \overrightarrow{stepsize_i}$$

Else

$$\overrightarrow{stepsize_i} = \left(\overrightarrow{Elite_i} - \vec{R}_B * \overrightarrow{Prey_i}\right) / \vec{R}_B, i = 1, \ldots n$$

$$\overrightarrow{Prey_i} = \overrightarrow{Prey_i} - P.\vec{R} * \overrightarrow{stepsize_i}$$

End;

Step 5: While $\frac{1}{3} Max\_Iter < Iter < \frac{2}{3} Max\_Iter$

For the first half of population;

If $R > 0.5$

$$\overrightarrow{stepsize_i} = \left(\overrightarrow{Elite_i} - \vec{R}_L * \overrightarrow{Prey_i}\right) * \vec{R}_L, i = 1, \ldots, {}^{n}/_{2}$$

$$\overrightarrow{Prey_i} = \overrightarrow{Prey_i} + P.\vec{R} * \overrightarrow{stepsize_i}$$

Else

$$\overrightarrow{stepsize_i} = \left(\overrightarrow{Elite_i} - \vec{R}_L * \overrightarrow{Prey_i}\right) / \vec{R}_L, i = 1, \ldots, {}^{n}/_{2}$$

$$\overrightarrow{Prey_i} = \overrightarrow{Prey_i} - P.\vec{R} * \overrightarrow{stepsize_i}$$

End;

Step 6: If $R > 0.5$

$$\overrightarrow{stepsize_i} = \left(\vec{R}_B * \overrightarrow{Elite_i} - \overrightarrow{Prey_i}\right) * \vec{R}_B \quad i = n/2, \ldots n$$

$$\overrightarrow{Prey_i} = \overrightarrow{Elite_i} + P.CF * \overrightarrow{stepsize_i}$$

Else

$$\overrightarrow{stepsize_i} = \left(\vec{R}_B * \overrightarrow{Elite_i} - \overrightarrow{Prey_i}\right) / \vec{R}_B \quad i = n/2, \ldots n$$

$$\overrightarrow{Prey_i} = \overrightarrow{Elite_i} - P.CF * \overrightarrow{stepsize_i}$$

End;

Step 7: While $Iter > \frac{2}{3} Max\_Iter$

If $R > 0.5$

$$\overrightarrow{stepsize_i} = \left(\vec{R}_L * \overrightarrow{Elite_i} - \overrightarrow{Prey_i}\right) * \vec{R}_L \quad i = 1, \ldots n$$

$$\overrightarrow{Prey_i} = \overrightarrow{Elite_i} + P.CF * \overrightarrow{stepsize_i}$$

Else

$$\overrightarrow{stepsize_i} = \left(\vec{R}_L * \overrightarrow{Elite_i} - \overrightarrow{Prey_i}\right) / \vec{R}_L \quad i = 1, \ldots n$$

$$\overrightarrow{Prey_i} = \overrightarrow{Elite_i} - P.CF * \overrightarrow{stepsize_i}$$

End;

Step 8: The final position updation is performed as shown in the following equ:

$$\overrightarrow{Prey_i} = \begin{cases} \overrightarrow{Prey_i} + CF\left[\vec{X}_{min} + \vec{R} * (\vec{X}_{max} - \vec{X}_{min})\right] * \vec{U} & if \ r \le FAD_S \\ \overrightarrow{Prey_i} + [FAD_S(1-r) + r]\left(\overrightarrow{Prey_{r1}} - \overrightarrow{Prey_{r2}}\right) & if \ r > FAD_s \end{cases}$$

Step 9: Repeat the above processes until reaching the stopping criterion;

Step 10: Return the best optimal solution;

### 3.4. Additional Noise Resistance Test

Around 3.27% of the data set, or 279 recordings, are under noisy class readings. This is a relatively minor fraction that can be readily eliminated. By introducing the various artificially generated intensities, the noise resistance of this model is examined. The original sample recording and the noise-corrupted versions are shown in Figure 5. Since there is no accurate estimation of the signal to noise ratio (SNR) for the available original noise recordings, original signals are assumed to be clean signals. Afterward, we compute $P_s$ using all of the energy from the original recordings and add white noise with a power of $P_n$. The Signal to Noise Ratio (SNR) is estimated based on the following model:

$$SNR = 10.log \frac{P_S}{P_n} dB \quad (13)$$

A training set has been generated using the feature values that were acquired for each level of noise. Separately, the test data set is not made publicly accessible. Therefore, k-fold cross-validation was used to evaluate the performance of classifiers (k = 10). The remaining 30% of each subset's data (N, A, and O) are reserved. Less than 70% of the data were used for training and validation. The results on the

remaining 30% of the data are shown to show the generalization capability. The averaged values are presented after each computation is run ten times on Matlab 2021a.

## 4. Results and Discussion

In this model, each recording undergoes pre-processing in order to produce the feature vector. From 0 Hz to 80 Hz, the power spectrum density and HRV-based properties are estimated. The pre-processing produced a feature vector of 41 dimensions. All of the top features under noise levels are HRV analysis descriptors that are almost linear. The signals were distorted at a high noise level (SNR = 10dB), which caused a small difference in the various rankings. As the noise level rises, the performance metrics fall. The findings from the top 10 features were contrasted with findings from all features as shown in Fig 4, which depicts the top-ranked features selected by the existing SVM, GA-SVM, MMF-SVM, and proposed MMPA-SVM techniques with respect to different SNR levels such as 10 dB, 20 dB, and 30 dB. Fig 5 validates the linear and non-linear characteristic analysis, where the inter-group comparisons are presented that includes the SD1, SD2, $AFE_V$, CDM and CCM.

| Rank | SNR_InfdB | SNR_30dB | SNR_20dB | SNR_10dB |
|---|---|---|---|---|
| 1 | {'AFEv' } | {'AFEv' } | {'AFEv' } | {'RR_mean' } |
| 2 | {'CCM' } | {'CCM' } | {'CCM' } | {'CCM' } |
| 3 | {'SD_ratio' } | {'SD_ratio' } | {'SD_ratio' } | {'SD_ratio' } |
| 4 | {'RR_mean' } | {'RR_mean' } | {'RR_mean' } | {'PSD_4.6-6.9' } |
| 5 | {'PSD_4.6-6.9' } | {'PSD_4.6-6.9' } | {'PSD_4.6-6.9' } | {'PSD_6.9-9.2' } |
| 6 | {'PSD_6.9-9.2' } | {'PSD_6.9-9.2' } | {'PSD_6.9-9.2' } | {'PSD_9.2-11.5' } |
| 7 | {'HANK_rr' } | {'HANK_rr' } | {'HANK_rr' } | {'PSD_2.3-4.6' } |
| 8 | {'PSD_9.2-11.5' } | {'PSD_9.2-11.5' } | {'PSD_9.2-11.5' } | {'PSD_11.5-13.8'} |
| 9 | {'PSD_11.5-13.8'} | {'PSD_11.5-13.8'} | {'PSD_11.5-13.8'} | {'AFEv' } |
| 10 | {'PSD_13.8-16.1'} | {'PSD_13.8-16.1'} | {'PSD_13.8-16.1'} | {'PSD_13.8-16.1'} |

(a). SVM

| Rank1 | SNR_InfdB1 | SNR_30dB1 | SNR_20dB1 | SNR_10dB1 |
|---|---|---|---|---|
| 1 | {'AFEv' } | {'AFEv' } | {'AFEv' } | {'RR_mean' } |
| 2 | {'CCM' } | {'SD_ratio' } | {'CCM' } | {'CCM' } |
| 3 | {'SD_ratio' } | {'CCM' } | {'HANK_rr' } | {'SD_ratio' } |
| 4 | {'RR_mean' } | {'RR_mean' } | {'SD_ratio' } | {'RR_STD' } |
| 5 | {'PSD_4.6-6.9' } | {'RR_STD' } | {'RR_mean' } | {'PSD_2.3-4.6' } |
| 6 | {'RR_STD' } | {'PSD_6.9-9.2' } | {'PSD_6.9-9.2' } | {'AFEv' } |
| 7 | {'PSD_6.9-9.2' } | {'HANK_rr' } | {'PSD_9.2-11.5' } | {'PSD_6.9-9.2' } |
| 8 | {'HANK_rr' } | {'PSD_9.2-11.5' } | {'PSD_11.5-13.8'} | {'PSD_9.2-11.5' } |
| 9 | {'PSD_9.2-11.5' } | {'PSD_11.5-13.8'} | {'PSD_13.8-16.1'} | {'PSD_2.3-4.6' } |
| 10 | {'PSD_11.5-13.8'} | {'PSD_2.3-4.6' } | {'PSD_16.1-18.4'} | {'PSD_11.5-13.8'} |

(b). GA-SVM

| Rank1 | SNR_InfdB1 | SNR_30dB1 | SNR_20dB1 | SNR_10dB1 |
|---|---|---|---|---|
| 1 | {'AFEv' } | {'AFEv' } | {'AFEv' } | {'RR_mean' } |
| 2 | {'CCM' } | {'SD_ratio' } | {'CCM' } | {'CCM' } |
| 3 | {'SD_ratio' } | {'CCM' } | {'SD_ratio' } | {'SD_ratio' } |
| 4 | {'RR_mean' } | {'RR_mean' } | {'HANK_rr' } | {'RR_STD' } |
| 5 | {'PSD_4.6-6.9' } | {'RR_STD' } | {'RR_mean' } | {'PSD_6.9-9.2' } |
| 6 | {'RR_STD' } | {'HANK_rr' } | {'PSD_6.9-9.2' } | {'PSD_2.3-4.6' } |
| 7 | {'HANK_rr' } | {'PSD_6.9-9.2' } | {'PSD_9.2-11.5' } | {'AFEv' } |
| 8 | {'PSD_6.9-9.2' } | {'PSD_9.2-11.5' } | {'PSD_11.5-13.8'} | {'PSD_9.2-11.5' } |
| 9 | {'PSD_9.2-11.5' } | {'PSD_11.5-13.8'} | {'PSD_13.8-16.1'} | {'PSD_2.3-4.6' } |
| 10 | {'PSD_11.5-13.8'} | {'PSD_2.3-4.6' } | {'PSD_16.1-18.4'} | {'PSD_11.5-13.8'} |

(c). MMF-SVM

| Rank | SNR_InfdB | SNR_30dB | SNR_20dB | SNR_10dB |
|---|---|---|---|---|
| 1 | {'AFEv' } | {'AFEv' } | {'AFEv' } | {'SD_ratio' } |
| 2 | {'CCM' } | {'SD_ratio' } | {'CCM' } | {'CCM' } |
| 3 | {'SD_ratio' } | {'CCM' } | {'RR_mean' } | {'AFEv' } |
| 4 | {'RR_mean' } | {'HANK_rr' } | {'SD_ratio' } | {'RR_mean' } |
| 5 | {'RR_STD' } | {'RR_mean' } | {'HANK_rr' } | {'PSD_6.9-9.2' } |
| 6 | {'PSD_4.6-6.9' } | {'RR_STD' } | {'PSD_6.9-9.2' } | {'PSD_2.3-4.6' } |
| 7 | {'HANK_rr' } | {'PSD_6.9-9.2' } | {'PSD_9.2-11.5' } | {'RR_STD' } |
| 8 | {'PSD_6.9-9.2' } | {'PSD_9.2-11.5' } | {'PSD_11.5-13.8'} | {'PSD_9.2-11.5' } |
| 9 | {'PSD_9.2-11.5' } | {'PSD_11.5-13.8'} | {'PSD_13.8-16.1'} | {'PSD_2.3-4.6' } |
| 10 | {'PSD_11.5-13.8'} | {'PSD_2.3-4.6' } | {'PSD_16.1-18.4'} | {'PSD_11.5-13.8'} |

(d). MMPA-SVM

**Fig 4.** Top ranked features selected by SVM, GA-SVM, MMF-SVM, and MMPA-SVM techniques

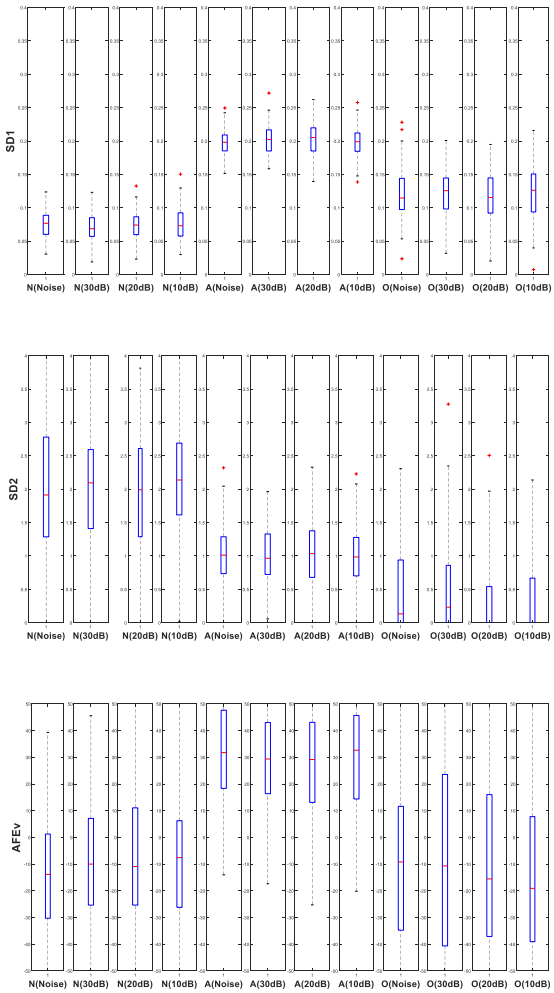

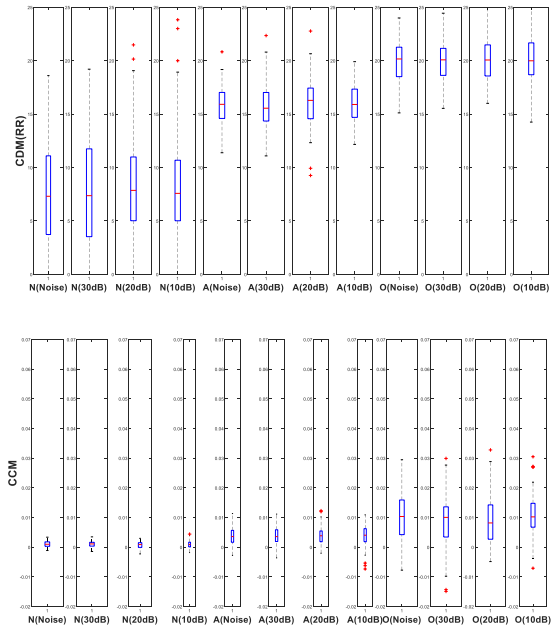


**Fig 5.** Linear and non-linear descriptor analysis

In this analysis, the suggested model is contrasted with various existing techniques, including SVM, GA-SVM, and MMF-SVM. These are all the common classification mechanisms based on meta-heuristic optimization that are used to identify AF from ECG signals. These methods also suffer from significant issues with training complexity, increased over-fitting, long training times, and slow convergence. With improved performance values, the suggested AAFD framework beats the other models. These outcomes were also contrasted with several classifiers from the literature. It has been found that MMPA performs better than other noise reduction methods and can be widely used in wearable technology. Sensitivity, specificity, and accuracy are the most popular parameters used to assess the performance of the classification techniques, which are computed by using the following equations:

$$Sen = \frac{TP}{TP+FN} \tag{14}$$

$$Spec = \frac{TN}{TN+FP} \tag{15}$$

$$Acc = \frac{TP+TN}{TP+TN+FP+FN} \tag{16}$$

Fig 6 and Fig 7 presents the comparative analysis among the existing SVM, GA-SVM, MMF-SVM, and proposed MMPA-SVM techniques with different classes such as Normal and Arrhythmia (NA), Others and Arrhythmia (OA), and Normal, Others, and Arrhythmia (NOA). The overall comparative analysis among the classification approaches under different configurations are illustrated in Table 3. For two-class classification issues, the MMPA-SVM classifier achieves the highest accuracy for N/A recordings when compared to both O/A and N/O recordings. Because nonlinear descriptors are sensitive to arrhythmias, it has been found that the N/A recordings with the highest accuracies—96.3%, 98.2%, 99.78% for SVM, GA-SVM, MMF-SVM, and MMPA-SVM, respectively—are achieved. The accuracy of MMPA-SVM is higher for all two-class classification tasks than for the other three classifiers when the findings of this work are compared with SVM, GA-SVM, and MMF-SVM classifiers. The accuracy decreases when the SNR is increased. The accuracy attained with all features is 99% for 10 dB SNR. The highest and lowest accuracy levels for N/A's top 10 features are 97.19% and 99.89%, respectively. Additionally, it has been found that categorization problems involving O/A and N/O result in a 5–10% reduction in accuracy. We defined A as a positive class, N and O as negative classes, and sensitivity & specificity equivalents as the quotient of true positive/negative cases and all positive/negative examples that were reported for the three-class classification issue. High specificities enable the best accuracy of 91.74% for N/O/A. Under all classifier configurations, the performance measures for this class problem gradually decline as the noise levels rise. Even after removing 80% of the low-ranked features and just taking into account the top 20% of features, the accuracy is identical. This supports our model-free, mutual information-based feature selection strategy. The computational impact and inference time in ECG are reduced when only the top 10 features are taken into account. We can therefore anticipate the implementation of this algorithm in wearable technology.

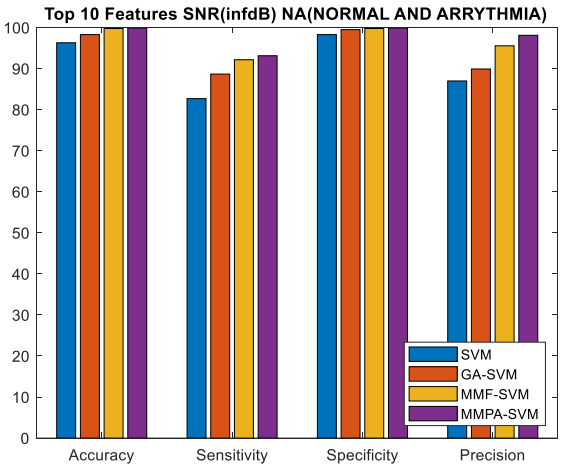


**Fig 6** (a). Comparative analysis based on the selected top 10 features with SNR (infdB) and NA

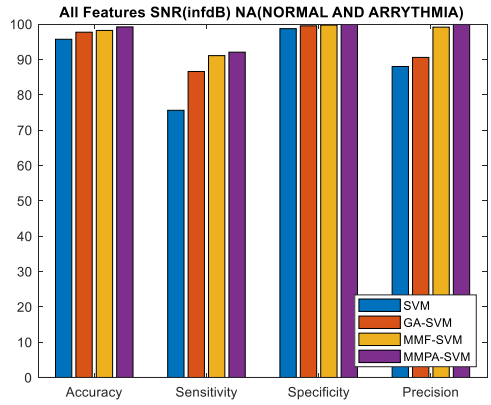


**Fig 6** (b). Comparative analysis with all features SNR (infdB) and NA

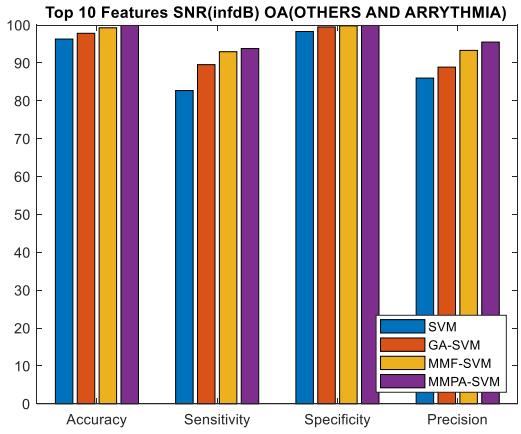


**Fig 6** (c). Comparative analysis based on the selected top 10 features with SNR (infdB) and OA

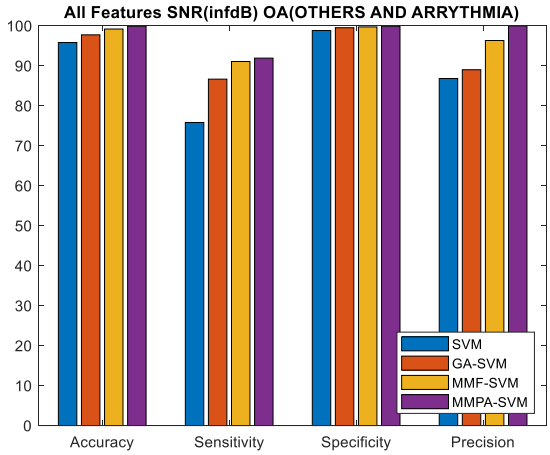


**Fig 6** (d). Comparative analysis with all features SNR (infdB) and OA

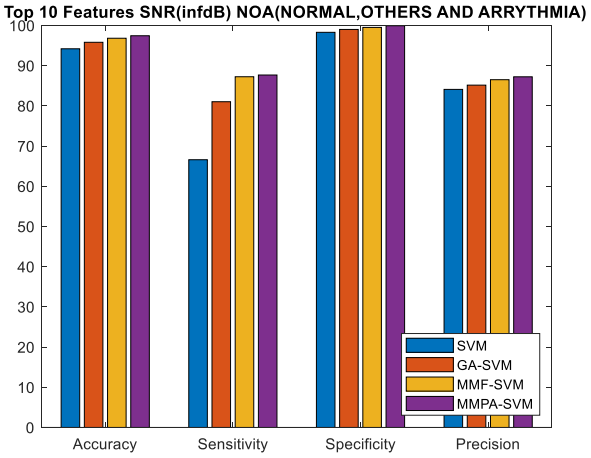


**Fig 7** (a). Comparative analysis based on the selected top 10 features with SNR (infdB) and NOA

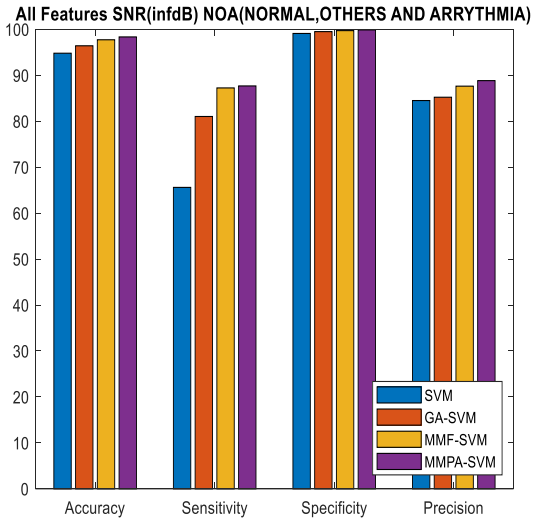


**Fig 7** (b). Comparative analysis with all features SNR (infdB) and NOA

**Table 1.** Overall comparative analysis under different SNR conditions

| | | N/A | | | O/A | | | N/O | | | N/O/A | | |
|---|---|---|---|---|---|---|---|---|---|---|---|---|---|
| SNR | FEATURES | CLASSIFIER | Acc | Sen | Spec | Acc | Sen | Spec | Acc | Sen | Spec | Acc | Sen | Spec |
| ∞dB | All | SVM | 95.77 | 75.66 | 98.67 | 89.66 | 69.77 | 98.99 | 83.44 | 62.66 | 93.33 | 80.44 | 65.66 | 98.82 |
| | | GA-SVM | 97.67 | 86.56 | 99.5 | 92.55 | 85.54 | 96.68 | 89.18 | 79.29 | 94.96 | 85.98 | 81.21 | 98.67 |
| | | MMF-SVM | 98.15 | 91.05 | 99.7 | 95.03 | 89.97 | 97.08 | 98.34 | 88.63 | 96.29 | 90.28 | 86.38 | 98.91 |
| | | MMPA-SVM | 99.12 | 92.14 | 99.8 | 95.99 | 90.81 | 97.87 | 93.35 | 89.32 | 99.95 | 90.87 | 86.90 | 99.39 |

| | | | | | | | | | | | | | |
|---|---|---|---|---|---|---|---|---|---|---|---|---|---|
| 30 dB | Top 10 | SVM | 96.3 | 82.7 | 98.3 | 89.6 | 74.9 | 94.3 | 80.3 | 60.8 | 89.6 | 78.2 | 73 | 97.3 |
| | | GA-SVM | 98.27 | 88.66 | 99.5 | 92.55 | 85.74 | 96.08 | 86.08 | 74.49 | 92.26 | 86.78 | 83.52 | 98.17 |
| | | MMF-SVM | 99.7 | 92.15 | 99.7 | 95.03 | 91.17 | 97.48 | 91.47 | 86.83 | 93.59 | 92.08 | 89.78 | 99.41 |
| | | MMPA-SVM | 99.8 | 93.11 | 99.89 | 95.99 | 92.01 | 98.27 | 92.25 | 87.52 | 94.25 | 92.67 | 90.30 | 99.8 |
| | All | SVM | 95.8 | 75.8 | 98.8 | 89.6 | 70 | 95.7 | 83 | 65.1 | 91.5 | 80.30 | 66.2 | 98.2 |
| | | GA-SVM | 97.72 | 86.55 | 99.5 | 92.18 | 85.58 | 97.27 | 88.51 | 80.55 | 92.95 | 85.57 | 81.45 | 98.36 |
| | | MMF-SVM | 99.18 | 90.93 | 99.88 | 94.47 | 90.27 | 98.55 | 92.77 | 86.77 | 94.17 | 87.70 | 86.58 | 98.44 |
| | | MMPA-SVM | 99.87 | 91.67 | 99.87 | 95.06 | 90.85 | 99.13 | 93.29 | 87.23 | 94.63 | 87.98 | 86.84 | 98.60 |
| 20 dB | Top 10 | SVM | 96.3 | 82.7 | 98.3 | 89.5 | 73.10 | 94.6 | 79.9 | 30 | 89.4 | 77.9 | 71.8 | 97.4 |
| | | GA-SVM | 97.82 | 89.45 | 99.42 | 93.08 | 86.68 | 96.17 | 90.41 | 75.45 | 91.85 | 88.17 | 87.05 | 98.06 |
| | | MMF-SVM | 99.2 | 92.83 | 99.78 | 95.37 | 89.97 | 97.45 | 93.67 | 87.07 | 93.07 | 92.30 | 91.18 | 98.54 |
| | | MMPA-SVM | 99.89 | 93.59 | 99.8 | 95.96 | 90.55 | 98.03 | 94.19 | 87.53 | 93.53 | 92.58 | 91.44 | 98.70 |
| | All | SVM | 95.7 | 75.10 | 98.8 | 89.5 | 69.10 | 95.9 | 83 | 65.7 | 91.2 | 80.20 | 65.10 | 98.3 |
| | | GA-SVM | 97.60 | 85.72 | 99.3 | 92.02 | 84.60 | 96.15 | 88.24 | 80.92 | 92.42 | 85.41 | 80.30 | 98.44 |
| | | MMF-SVM | 99.05 | 90.04 | 99.63 | 95.29 | 88.85 | 91.82 | 92.37 | 86.03 | 93.53 | 90.52 | 86.41 | 99.02 |
| | | MMPA-SVM | 99.96 | 90.67 | 99.8 | 95.82 | 89.36 | 97.53 | 92.62 | 86.25 | 93.75 | 90.74 | 86.62 | 99.16 |
| | Top 10 | SVM | 96 | 81.6 | 98.2 | 88.9 | 72.7 | 94 | 79.70 | 59.9 | 89.2 | 77.4 | 70.8 | 97.10 |
| | | GA-SVM | 97.90 | 87.22 | 98.95 | 92.42 | 88.20 | 95.25 | 89.94 | 79.12 | 91.42 | 87.6 | 81 | 98.04 |
| | | MMF-SVM | 99.15 | 91.54 | 99.63 | 93.69 | 91.45 | 96.38 | 93.07 | 89.73 | 93.53 | 89.72 | 86.11 | 98.72 |
| | | MMPA-SVM | 99.89 | 92.17 | 99.89 | 94.22 | 91.99 | 96.63 | 93.32 | 89.95 | 93.75 | 89.94 | 86.32 | 98.86 |

## 5. Conclusion

The innovative contribution of the proposed study is the development of a competent and highly efficient methodology for detecting AF from the available ECG signals. The HRV-based feature extraction methodology has been used in this framework to assess the dynamic features of the heart activity. The high level of robustness of the HRV model helps to increase the confidence and precision of detection. Additionally, the best features from the collection of available features are selected using the MMPA, which improves training rates and reduces classification false prediction rates. Then, an enhanced SVM model is utilized to precisely detect the AF using the refined set of traits. The suggested AAFD algorithm may identify AF even in brief ECG recordings. This algorithm outperforms the prototype in terms of accuracy and specificity, making it a contender for first screening. The usefulness of the HRV-based nonlinear features utilized for AF identification with brief ECG recordings is well-supported by this research work. Cascading classification may be a focus of future research given the prevalence of arrhythmias other than AF.

## References


[1] B. Tutuko, M. N. Rachmatullah, A. Darmawahyuni, S. Nurmaini, A. E. Tondas, R. Passarella, *et al.*, "Short single-lead ECG signal delineation-based deep learning: implementation in automatic atrial fibrillation identification," *Sensors*, vol. 22, p. 2329, 2022.

[2] Y. Jin, C. Qin, J. Liu, K. Lin, H. Shi, Y. Huang, *et al.*, "A novel domain adaptive residual network for automatic atrial fibrillation detection," *Knowledge-Based Systems*, vol. 203, p. 106122, 2020.

[3] Y. Chen, C. Zhang, C. Liu, Y. Wang, and X. Wan, "Atrial Fibrillation Detection Using a Feedforward Neural Network," *Journal of Medical and Biological Engineering*, vol. 42, pp. 63-73, 2022.

[4] F. Murat, F. Sadak, O. Yildirim, M. Talo, E. Murat, M. Karabatak, *et al.*, "Review of deep learning-based atrial fibrillation detection studies," *International journal of environmental research and public health*, vol. 18, p. 11302, 2021.

[5] Y. Liu, J. Chen, N. Bao, B. B. Gupta, and Z. Lv, "Survey on atrial fibrillation detection from a single-lead ECG wave for Internet of Medical Things," *Computer Communications*, vol. 178, pp. 245-258, 2021.

[6] X. Chen, Z. Cheng, S. Wang, G. Lu, G. Xv, Q. Liu, *et al.*, "Atrial fibrillation detection based on multi-feature extraction and convolutional neural network for processing ECG signals," *Computer Methods and Programs in Biomedicine*, vol. 202, p. 106009, 2021.

[7] S. Ummadisetty and M. Tatineni, "Automatic Atrial Fibrillation Detection Using Modified Moth Flame

Optimization Algorithm," *International Journal of Intelligent Engineering & Systems,* vol. 16, 2023.

[8] O. E. Santala, J. Halonen, S. Martikainen, H. Jäntti, T. T. Rissanen, M. P. Tarvainen, *et al.*, "Automatic mobile health arrhythmia monitoring for the detection of atrial fibrillation: prospective feasibility, accuracy, and user experience study," *JMIR mHealth and uHealth,* vol. 9, p. e29933, 2021.

[9] J. Rahul and L. D. Sharma, "Artificial intelligence-based approach for atrial fibrillation detection using normalised and short-duration time-frequency ECG," *Biomedical Signal Processing and Control,* vol. 71, p. 103270, 2022.

[10] Y. Ping, C. Chen, L. Wu, and M. Shu, "Automatic atrial fibrillation detection based on deep learning model with shortcut connection," in *2020 IEEE 5th Information Technology and Mechatronics Engineering Conference (ITOEC)*, 2020, pp. 1075-1079.

[11] S. Mousavi, F. Afghah, and U. R. Acharya, "HAN-ECG: An interpretable atrial fibrillation detection model using hierarchical attention networks," *Computers in biology and medicine,* vol. 127, p. 104057, 2020.

[12] T. Mahmud, S. A. Fattah, and M. Saquib, "Deeparrnet: An efficient deep cnn architecture for automatic arrhythmia detection and classification from denoised ecg beats," *IEEE Access,* vol. 8, pp. 104788-104800, 2020.

[13] G. G. Geweid and J. D. Chen, "Automatic classification of atrial fibrillation from short single-lead ECG recordings using a Hybrid Approach of Dual Support Vector Machine," *Expert Systems with Applications,* vol. 198, p. 116848, 2022.

[14] N. Ganapathy, D. Baumgärtel, and T. M. Deserno, "Automatic detection of atrial fibrillation in ECG using co-occurrence patterns of dynamic symbol assignment and machine learning," *Sensors,* vol. 21, p. 3542, 2021.

[15] Y. Liu, J. Chen, B. Fang, Y. Chen, and Z. Lv, "Ensemble Learning-Based Atrial Fibrillation Detection From Single Lead ECG Wave for Wireless Body Sensor Network," *IEEE Transactions on Network Science and Engineering,* 2022.

[16] G. Tuboly, G. Kozmann, O. Kiss, and B. Merkely, "Atrial fibrillation detection with and without atrial activity analysis using lead-I mobile ECG technology," *Biomedical Signal Processing and Control,* vol. 66, p. 102462, 2021.

[17] Z. Ebrahimi, M. Loni, M. Daneshtalab, and A. Gharehbaghi, "A review on deep learning methods for ECG arrhythmia classification," *Expert Systems with Applications: X,* vol. 7, p. 100033, 2020.

[18] J. Wang, "An intelligent computer-aided approach for atrial fibrillation and atrial flutter signals classification using modified bidirectional LSTM network," *Information Sciences,* vol. 574, pp. 320-332, 2021.

[19] C. Chen, Z. Hua, R. Zhang, G. Liu, and W. Wen, "Automated arrhythmia classification based on a combination network of CNN and LSTM," *Biomedical Signal Processing and Control,* vol. 57, p. 101819, 2020.

[20] P. Pławiak and U. R. Acharya, "Novel deep genetic ensemble of classifiers for arrhythmia detection using ECG signals," *Neural Computing and Applications,* vol. 32, pp. 11137-11161, 2020.

[21] F. Murat, O. Yildirim, M. Talo, U. B. Baloglu, Y. Demir, and U. R. Acharya, "Application of deep learning techniques for heartbeats detection using ECG signals-analysis and review," *Computers in biology and medicine,* vol. 120, p. 103726, 2020.

[22] A. Ukil, L. Marin, S. C. Mukhopadhyay, and A. J. Jara, "AFSense-ECG: Atrial fibrillation condition sensing from single lead electrocardiogram (ECG) signals," *IEEE Sensors Journal,* vol. 22, pp. 12269-12277, 2022.

[23] N. Ahmed and Y. Zhu, "Early detection of atrial fibrillation based on ECG signals," *Bioengineering,* vol. 7, p. 16, 2020.

[24] P. Lyakhov, M. Kiladze, and U. Lyakhova, "System for Neural Network Determination of Atrial Fibrillation on ECG Signals with Wavelet-Based Preprocessing," *Applied Sciences,* vol. 11, p. 7213, 2021.

[25] J. Wang, "Automated detection of atrial fibrillation and atrial flutter in ECG signals based on convolutional and improved Elman neural network," *Knowledge-Based Systems,* vol. 193, p. 105446, 2020.